HHS Public Access

Author manuscript

Matter. Author manuscript; available in PMC 2023 February 02.

Published in final edited form as:

Matter. 2022 February 02; 5(2): 666–682. doi:10.1016/j.matt.2021.11.017.

Immunomodulatory Microneedle Patch for Periodontal Tissue Regeneration

Xuexiang Zhang[1,§], **Mohammad Mahdi Hasani-Sadrabadi**[1,§], **Jana Zarubova**[1], **Erfan Dashtimighadam**[2], **Reihaneh Haghniaz**[1,3], **Ali Khademhosseini**[1,3], **Manish J. Butte**[4,5], **Alireza Moshaverinia**[6], **Tara Aghaloo**[7], **Song Li**[1,*]

[1]Department of Bioengineering, University of California, Los Angeles, CA 90095, United States

[2]Department of Chemistry, University of North Carolina at Chapel Hill, Chapel Hill, NC, 27599-3290 United States

[3]Terasaki Institute for Biomedical Innovation, Los Angeles, CA, 90064 USA

[4]Department of Pediatrics, Division of Immunology, Allergy, and Rheumatology, University of California Los Angeles, Los Angeles, CA 90095, United States

[5]Department of Microbiology, Immunology, and Molecular Genetics, University of California Los Angeles, Los Angeles, CA 90095, USA

[6]Weintraub Center for Reconstructive Biotechnology, Division of Advanced Prosthodontics, School of Dentistry, University of California, Los Angeles, California 90095, United States

[7]Division of Diagnostic and Surgical Sciences, School of Dentistry, University of California, Los Angeles, Los Angeles, CA 90095, United States

SUMMARY

Periodontal diseases are caused by microbial infection and the recruitment of destructive immune cells. Current therapies mainly deal with bacteria elimination, but the regeneration of periodontal tissues remains a challenge. Here we developed a modular microneedle (MN) patch that delivered both antibiotic and cytokines into the local gingival tissue to achieve immunomodulation and tissue regeneration. This MN patch included a quickly dissolvable gelatin membrane for an immediate release of tetracycline and biodegradable GelMA MNs that contained tetracycline-loaded poly(lactic-co-glycolic acid) nanoparticles and cytokine-loaded silica microparticles for a sustained release. Antibiotic release completely inhibited bacteria growth, and the release

[*]Corresponding Author: songli@ucla.edu (S.L.). Lead Contact: Song Li (songli@ucla.edu).
[§]Equal contribution

Author Contributions: X.Z., M.M.H.-S., and S.L. conceived the presented idea and designed experiments. X.Z. and M.M.H.-S., performed experiments, analyzed the data and wrote the paper. J.Z. and R.H. contributed to some in vitro experiments. E.D. contributed to animal experiments. All authors edited the manuscript.

Declaration of Interests: S.L., M.M.H.-S., T.A., and A.M. have patent applications (periodontal micropatch and uses thereof, U.S. Provisional Patent Application PCT/US20/58069) related to the current study and, thus, may have related financial interests. The other authors declare no potential conflicts of interest with respect to the authorship and/or publication of this article.

of IL-4 and TGF-β induced the repolarization of anti-inflammatory macrophages and the formation of regulatory T cells *in vitro*. *In vivo* delivery of MN patch into periodontal tissues suppressed proinflammatory factors and promoted pro-regenerative signals and tissue healing, which demonstrated the therapeutic potential of local immunomodulation for tissue regeneration.

eTOC blurb

Periodontitis is a chronic inflammatory disease causing the degeneration of tooth-supporting tissues in humans. Besides bacterial infection, destructive immune cells play a critical role in the tissue loss. To address the challenge of drug delivery in oral cavity and achieve periodontal tissue regeneration, we engineer an immunomodulatory microneedle patch to enable minimally invasive tissue penetration and local retention for a sustained delivery of antibiotics and cytokines that promotes pro-regenerative signals locally.

Graphical Abstract

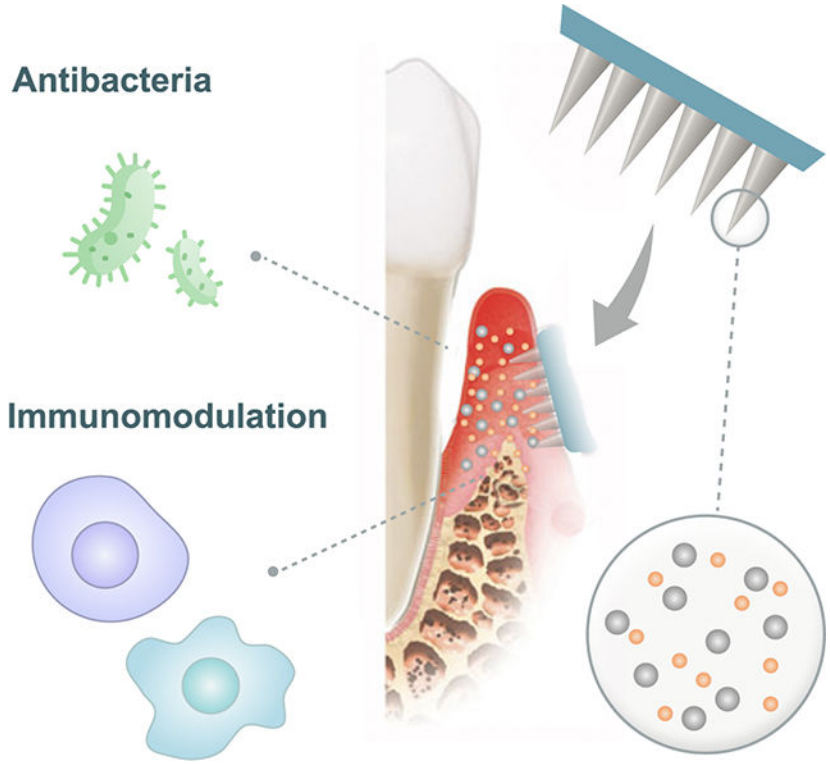

Keywords

Microneedles; biomaterials; immunoengineering; local immunomodulation; anti-bacteria; anti-inflammatory

INTRODUCTION

Periodontitis is one of the most common diseases of mankind, and approximately 50% of the American population has some degree of periodontal diseases[1]. It is a prevalent

chronic destructive inflammatory disease affecting tooth-supporting tissues in humans[2]. The bacterial colonization of the periodontal pocket and the inflammatory responses of the host collaboratively cause periodontitis. As the disease progresses, tissue inflammation leads to progressive periodontal detachment and the degeneration of the periodontium, including periodontal ligament, and root cementum, alveolar bone, which may eventually lead to early tooth loss[1–3].

Antibiotics have been administered in many forms and formulations as a conventional strategy to combat bacterial infection. Oral administration of antibiotics requires large dosages to reach the effective level at the diseased site. Local administration using biodegradable materials such as poly(lactic-co-glycolic acid) (PLGA) nanoparticles (NPs) can achieve a prolonged release[4,5], but has little effect on periodontal tissue regeneration. Furthermore, none of the existing regenerative treatments directly addresses the problem of inflammatory immune cells in the periodontal microenvironment.

Although microbial infection is the fundamental cause of the periodontitis, the accumulation of destructive immune cells such as macrophages plays a critical role in the periodontitis progression[6,7]. Secretion of inflammatory cytokines and proteases accelerates gingival tissue degeneration, alveolar bone resorption, and periodontal connective tissue damage[6–9]. In addition to macrophages, helper T cells also respond to the micro-immune environment and contribute adversely to the accumulation of inflammatory cytokines and chemokines[10]. We hypothesized that a conversion of inflammatory M1 macrophages and T cells into anti-inflammatory M2 macrophages and T regulatory cells (Tregs) could create a pro-healing microenvironment for periodontal tissue regeneration. It has been shown that cytokines such as interleukin 4 (IL-4) can induce the conversion of macrophages from M1 to M2 type to enhance tissue regeneration[11–13]. In addition, IL-4 can control inflammation by differentiating naïve T cell into induced regulatory T cells (Treg) in the presence of transforming growth factor β (TGF-β), which also helps repolarize macrophages toward anti-inflammatory (M2) lineages (Figure S1)[14]. It is worth noting that IL-4, as determined by meta-analysis, is the only cytokine that decreases in chronic periodontitis patients and increases after periodontal treatment[15,16]. Furthermore, IL-4 can downregulate proinflammatory cytokines[17] and restrain osteoclastogenesis[18,19].Therefore, we investigated whether a sustained delivery of IL-4 and TGF-β was sufficient to modulate macrophages and T cells for periodontal tissue regeneration.

Drug delivery in the oral cavity is challenging due to bacterial infection, saliva secretion and poor local retention. To address this challenge and achieve local and sustained drug delivery, we have developed a biodegradable microneedle (MN) patch that can be inserted into the pocket between the tooth and gingival tissue for a painless and suture-free placement into the gingival tissue (Figure 1a). For a human patient with severe periodontitis, MN patch can be inserted immediately after scaling and root planning procedure by dentists or hygienists. For less severe periodontitis or gingivitis, MN patch may be placed on the outer surface of the gingiva by patients themselves. This MN patch offers penetration through the gingival tissue and leaves bullets of MNs inside for a sustained delivery of antibiotics and immunomodulatory cytokines. Although MN patches have been employed for transdermal, ocular, vascular and mucosal drug deliveries[20,21], MNs are generally used to deliver a single

therapeutic, and there is a lack of a flexible modular design for a controlled delivery of multiple therapeutics at different rates. Here we design a modular MN patch for a multiplex delivery: (1) the base membrane of the MN patch is dissolvable for a burst release of antibiotics, (2) biodegradable NPs in MNs offers a sustained delivery of antibiotics, and (3) heparin-coated mesoporous silica microparticles (SiMPs) are used as carriers to maintain protein stability[22] and ensure a prolonged delivery of IL-4 and TGF-β. This modular MN patch can be easily adopted for various multiplex drug delivery applications. In this study, we explored its application for a multiplex delivery of antibiotic and immunomodulatory cytokines to promote periodontal tissue regeneration.

RESULTS

Design and fabrication of periodontal MN patch.

We designed and fabricated the MN patch with two parts: a dissolvable base membrane and MNs loaded with NPs and SiMPs (Figure 1b). The supporting base membrane is made of 10% gelatin, which solidifies at room temperature and is dissolvable at body temperature. Antibiotics can be loaded directly into the gelatin membrane and released quickly regardless of the crosslinking state of gelatin. To achieve a burst release with a simple patch design, we did not crosslink the gelatin membrane, which allowed the membrane to be dissolved within minutes. The MNs are made of gelatin methacryloyl (GelMA) crosslinked by UV light. This crosslinked GelMA network does not dissolve immediately but forms a hydrogel structure that degrades over time. The hydrogel holds drug carriers (NPs and SiMPs) in place and allows released therapeutic agents passing through its porous structure. Detailed synthesis and properties of GelMA can be found in our previous publication[23]. After applying MN patch to gingival tissue, the base membrane dissolves quickly for a burst release of antibiotics to immediately reduce bacterial content in the microenvironment, while the biocompatible and bioresorbable MNs penetrate and stay in gingival tissue for a sustained release of antibiotics and cytokines.

For the selection of active ingredients in the formulation, a commonly used antibiotic tetracycline was selected as a model drug, which was loaded into the gelatin base for a burst release and NPs in MNs for a sustained release. IL-4 and TGF-β were loaded into heparin-SiMPs and encapsulated in GelMA MNs. IL-4 and TGF- β have isoelectric points of 9.17 and 8.83, respectively at physiological pH. Enhanced affinity of IL-4 and TGF- β toward PEG-heparin[24] and alginate-heparin [25] based hydrogels has been reported before. Here, negatively charged heparin modified SiMPs can also interact strongly with these cytokines not only to prolong their release but also to protect them from denaturation during the MN fabrication.

The fabrication process is illustrated in Figure S2. To fabricate MNs, 20% (w/v) GelMA containing photoinitiator, tetracycline-loaded NPs and IL-4/TGF-β loaded SiMPs were cast on negative MN molds and centrifuged to fill the molds. The extra mixture was removed, and 10% gelatin containing 5mg/ml of tetracycline-HCl was laid evenly on the top of the mold to create a patch. The MN patches were peeled off from the mold following UV irradiation followed by drying at room temperature. UV light exposure did not cause significant changes of protein stability as the release of IL-4 from MNs with and without UV

exposure had similar effects on the gene expression of phenotypic markers in macrophages (Figure S3).

Physical characterization and mechanical property of MN patch.

As shown in electron microscopy images, the resulting MNs were conical, with a base diameter of 300 μm, a height of 600 μm and a tip diameter of ~15 μm (Figure 1 c,d). SiMPs accumulated more at the tips of the needle after centrifugation, and roughly occupied 15% of the needle volume due to their high density. Using green fluorescence-labeled NPs and red fluorescence-labeled SiMPs, the distribution of particles in MNs can be seen from the fluorescent images in Figure 1e.

The mechanical property of MNs is critical for gingival tissue penetration. We performed compression test of MNs with and without NPs or SiMPs. Adding NPs did not significantly affect the mechanical property of MNs, but the addition of SiMPs to MNs strengthened the mechanical strength by two folds (Figure 1f). These composite MNs had sufficient mechanical strength to penetrate the freshly extracted pig or rat gingival tissues (Figure 1g,h,i). Slight swelling was observed when MNs were in contact with phosphate-buffered saline (PBS) (Figure S4). The degradation rate of the GelMA MNs were characterized in physiologically relevant solutions (Figure 1j). UV-crosslinked GelMA MNs were degraded by half in PBS with collagenase after 5 days. MN degradation was slightly slower in human saliva (Figure 1j), which might be accelerated in the acidic environment at the disease sites of periodontitis. In addition, a standard sterilization of MN patches with x-ray irradiation did not change the physical properties of patches (Figure S5).

Delivery of antibiotics by periodontal MN patch and antibacterial effects *in vitro*.

We designed periodontal MN patch to deliver antibiotics in two stages: first, a burst release during the dissolution of patch base (gelatin), and second, a sustained delivery by PLGA NPs embedded in GelMA MNs. Due to the hydrophobicity of tetracycline, tetracycline-HCl was used for the patch base formulation as it is more water-soluble. As the gelatin base melt at 37°C in an aqueous environment, the release of tetracycline from the gelatin base was linear and the whole base disappeared after ~10 minutes, shown in Figure 1k. For PLGA NPs synthesis, tetracycline was dissolved in organic solvent and NPs were synthesized by ultrasonication. The loading efficiency was calculated to be around 70%, and the particle sizes had a relatively uniform distribution around 150 nm (Figure S6). Inclusion of antibiotic in both gelatin base and encapsulated PLGA NPs provided sustained and prolonged release profiles (Figure 1l).

Antibacterial properties of designed patches were evaluated on a standard bacterium, *E.Coli*, as well as clinically pathogenic bacteria *P.gingivalis* (*P.g.*) by using agar-plate and liquid cultures, respectively. We performed antibacterial tests to examine the effects of MN patch-released tetracycline on bacterial growth both on the surface and in solution. Tetracycline released from MN patch had a strong antibacterial activity as assessed by estimating the inhibition zone (Figure S7). Consistent bacteria-killing of periodontal disease-causing bacteria *P.g.* was also observed in liquid culture (Figure 1m). While NP-released tetracycline partially inhibited *P.g.* growth, the full patch was able to inhibit *P.g.* growth completely.

These results demonstrated the successful loading of tetracycline into gelatin base and encapsulation of tetracycline into PLGA NPs in MNs for effective bacterial killing.

To enable a prolonged release of cytokines, we made monodisperse mesoporous SiMPs (~15 μm diameter and ~10 nm pore size) (Figure 2a) *via* a microfluidic jet spray-drying route as reported before.[26,27] Carbodiimide chemistry was utilized to modify SiMPs with heparin to improve the loading and activity maintenance of cytokines (Figure 2b–c). *In vitro* degradation of heparin-functionalized SiMPs indicated that these particles were mostly degraded in two weeks (Figure 2d). The presence of heparin ensured the efficient loading and the prolonged release of IL-4 and TGF-β (Figure 2e–f).

Anti-inflammatory properties of periodontal MN patch *in vitro*.

To investigate whether the encapsulated cytokines were functional after SiMPs were cast into MNs, MN patches with cytokine-loaded SiMPs were placed in culture wells for a co-culture with murine bone marrow-derived macrophages (BMDMs). Macrophages are known for their plasticity to switch between proinflammatory M1 and pro-healing M2 macrophages. The macrophages can be preferentially induced to produce either inducible nitric oxide synthase (iNOS) (M1 marker) or ariginase-1 (ARG-1) (M2 marker); in addition, M1 macrophages produce inflammatory cytokines like interleukin 1β (IL-1β), and M2 macrophages upregulate mannose receptor C-type 1 (MRC1).[12,28,29] Therefore, we examined the expression of these biological markers to characterize the status of macrophage repolarization. Figure 3a demonstrates a sustained release of IL-4 from MN patches over time. Co-culture of IL-4-releasing MN patches with BMDMs that were pre-treated with lipopolysaccharide (LPS) (Figure 3b) significantly suppressed the expression of proinflammatory genes such as iNOS and IL-1β while inducing anti-inflammatory genes such as MRC1 and ARG-1 (Figure 3c). Consistently, the secretion level of inflammatory cytokines such as IL-1β into the cell culture media significantly decreased (Figure S8). In addition, when IL-4-releasing MN patches were placed in Transwells for a no-contact co-culture with BMDMs, the same effects on pro-inflammatory and anti-inflammatory genes were observed (Figure S9). These results demonstrated the maintenance of IL-4 activity during MN fabrication and the immunomodulatory effects of released IL-4 on macrophages.

The presence of TGF-β during T cell activation can induce the formation of Treg [30,31]. SiMPs loaded with TGF-β were encapsulated into MNs and showed a sustained release profile (Figure 3d). To determine the effects of the sustained presentation of IL-4 and TGF-β on Treg formation, we incubated primary murine $CD4^+$ (helper) T cells with activation signals (anti-CD3 and anti-CD28 antibodies) in the presence of IL-4/TGF-β-loaded MN patches. Indeed, the sustained release of IL-4 and TGF-β significantly induced Treg formation, which was more effective than adding the soluble form of IL-4 and TGF-β in culture media (Figure 3e).

In vivo studies of MN patches for periodontitis treatment.

The functionality of the designed MN patch was tested *in vivo* by using a rat model of periodontitis. Following the periodontal disease induction, MN patches were inserted in

the periodontal pocket to assess immunomodulation and tissue regeneration at cellular and tissue levels.

To better understand the mechanism of action, we extracted the periodontal tissues at the defect site to assess the population and status of local immune cells (Figure 4a). As the disease was induced by *Aggregatibacter actinomycetemcomitans* (*A.a.*) bacterial coated ligatures, we first assess the presence of bacteria by using quantitative polymerase chain reaction (qPCR). As shown in Figure 4b, therapeutic patches effectively inhibited the bacterial growth by the two-staged release of tetracycline. In addition, the level of pro-inflammatory cytokines such as tumor necrosis factor α (TNF-α; both mRNA and protein level, Figure 4c–d), IL-1β and IFN-γ (**Figure 10**) was significantly reduced in the presence of therapeutic patches that delivered both immunoregulatory cytokines and antibiotics. Treatment with therapeutic patches not only decreased the inflammatory cytokines, but also increased the expression of anti-inflammatory cytokine such as IL-10 (both mRNA and protein level, Figure 4e–f), Treg marker, FOXP3 (Figure 4g) and Treg stimulating factor, TGF-β (Figure 4g). Furthermore, therapeutic MN patches induced pro-healing genes, including RUNX2, COL1A1 (type I collagen α1), BMP-2, and OCN (osteocalcin) (Figure 4h), indicating an induction of osteogenic activity and collagen matrix synthesis in local periodontal cells.

Following the periodontal disease induction, MN patches were inserted in the periodontal defect pocket in a way for needles to face the gum tissue (Figure 5a). Four- and Eight-weeks post-treatment, saliva samples were extracted to check the level of inflammatory cytokines (Figure 5b). Consistent with the findings in periodontal tissues, the saliva from the rats treated with therapeutic patches showed a significant reduction in the secretion level of IL-1β and TNF-α, two major pro-inflammatory cytokines.

Eight weeks post-insertion, the bone regeneration at the defect site was assessed by using microcomputed tomography (μCT). Reconstructed two-dimensional (2D) and 3D images of the defect site following various treatments are exemplified in Figure 5c. These μCT images were then used to estimate the level of alveolar bone gain at each defect site. The rats treated with therapeutic patches had a significant reduction in the distance between the alveolar bone crest and cementoenamel junction (CEJ) and an increase of alveolar bone area, which was not observed in animals treated with blank patches (Figure 5d). Although the recovered bone area is not as good as healthy control but such a significant improvement only after eight weeks of treatment is among the highest reported in the literature.[32–34]

DISCUSSION

Periodontitis is a prevalent chronic inflammatory disease affecting tooth-supporting tissues. Although bacterial colonization of the periodontal pocket is the initial cause of the periodontitis, accumulation of destructive immune cells such as macrophages and T cells into the periodontium plays a critical role in the disease progression. Once damaged, the periodontium has a limited capacity for regeneration. Thus, the ultimate goal of periodontal therapy is the regeneration of the periodontium. With conventional administration, insufficient local presentation of antibiotics and inadequate penetration of

anti-inflammatory drugs across the transgingival layers as well as not considering the critical role of immune cells, limiting the therapeutic outcome. Therefore, the local modulation of the microbial environment and immune microenvironment with good tissue penetration is desirable.

Our patch offers four tunable modules – dissolvable base, MN arrays, NPs and SiMPs, which can be engineered to have different active pharmaceutical ingredients, and the biomaterials for each module can be further tuned to have the desirable release and degradation profile. Therefore, our patch is not only appropriate for the therapy of gingivitis and periodontitis, but also for other problems in the oral cavity, such as canker sores when loading with a different drug. During the MN fabrication process, we observed that SiMPs had intendency to settle near the tip of the MNs. Interestingly, we found that the accumulation of microparticles at the tip of the needles help increase tip strength (Fig. 1f) for tissue penetration. We believe that this design will enhance the effective delivery of immunomodulatory molecules. On the other hand, if the even distribution of SiMPs is desirable, smaller particles could be used so that they would not precipitate much during centrifugation steps. In addition, surface modification of particles may increase the active interaction with the surrounding matrix to achieve a homogenous distribution of particles.

To achieve an easy-to-administer and highly effective periodontal therapy, this study tuned the modules and developed a MN patch with biodegradable MNs and dissolvable support upon application to the gingival tissue. Tetracycline is used as a model drug in our periodontal patch and it can be replaced or combined with other clinically relevant antibiotics, such as minocycline, azithromycin, metronidazole and ciprofloxacin.[35] Antibiotic-loaded PLGA NPs as well as cytokine-loaded mesoporous SiMPs control the release of active ingredients and protect the integrity of biomolecules. This design enables multi-stage release: a burst release of antibiotics from the base membrane and a sustained release of more antibiotics from MPs, as well as immunomodulatory cytokines, IL-4 and TGF-β, from SiMPs in MNs, to suppress bacteria growth and to modulate host immune cell functions, respectively. This is the first-in-class periodontal drug delivery system with both antibacterial and immunomodulatory effects in the same patch.

Maintaining the stability and integrity of protein is crucial for delivering functional immunomodulatory cytokines and achieving effective immune modulation. Here, heparin-functionalized particles (i.e., SiMPs) can interact with the potential cytokines and stabilize them through electrostatic interaction and heparin-specific binding. An alternative approach is to directly use heparin-functionalized hydrogel to make MNs for the loading and release of cytokines and growth factors. However, the fabrication of MNs involve processes such as crosslinking and drying to achieve a sufficient mechanical strength, which may compromise the bioactivity of biomolecules. Therefore, the successful loading of a biomolecule and the preservation of its activity require biomolecule-specific test and optimization to determine the feasibility.

Finally, following the successful demonstration of immunomodulation approach, further optimization and simplification of the MN patch is required for clinical translation in dental applications. For example, instead of protein-based cytokines, small molecules capable of

tuning macrophages into pro-healing phenotype may be desirable because of their better stability, easier manufacturing procedure and lower cost. Our future goal is to develop a point of care product for patients to administer easily without frequent visits to dentists and complicated surgical procedures. Over-the-counter products will further grant patients the freedom to self-educate and diagnose, thus starting treatment intervention from the early stages of periodontitis. The commercialization potential will be huge with simplified formulation and optimized materials.

EXPERIMENTAL PROCEDURES

Resource availability.

Lead contact: Song Li (songli@ucla.edu)

Materials availability: This study did not generate new unique materials.

Data and code availability: All data associated with this study are present in the paper or the Supplemental Information. Raw data are available upon request.

Chemicals and biologicals.

Unless noted otherwise, all chemicals were purchased from Sigma-Aldrich, Inc. Glassware was acid-cleaned overnight and then thoroughly rinsed with Milli-Q water. Cell culture reagents, solutions, and dishes were obtained from Thermo Fisher Scientific Corp. unless otherwise specified.

GelMA synthesis.

GelMA was prepared as previously described[23]. Briefly, 10 g of porcine skin gelatin was dissolved in 100 mL of preheated Millipore water at 60°C under constant stir. Fully dissolved gelatin solution was filtered through a membrane with 0.22 μm pore size. The filtered 10% gelatin could be used for MN patch base material as well as GelMA synthesis. Keeping the solution temperature around 50°C, 8 mL of methacrylic anhydride was added to the stirring mixture dropwise and the reaction was carried for 3 hours. To stop the reaction, a five-fold volume of warm water was added to the solution. Residual monomers and methacrylic anhydride were removed by dialysis with 12–14 kDa molecular weight cut-off dialysis tubing at 40°C for one week. GelMA polymer solution was freeze-dried and stored in 4°C fridge.

PLGA nanoparticle synthesis.

200 mg acid terminated PLGA (50:50 lactic acid to glycolic acid ratio) was dissolved and stirred in 5 ml dichloromethane (DCM) overnight on heat. For tetracycline loaded into NPs, 15 mg tetracycline was added to 5 ml of PLGA-DCM mixture. A ten-fold volume of 1% polyvinyl alcohol (PVA) was added right before sonication at 40% power for 2 minutes with 4-second on and 2-second off cycle. The sonicated solution was poured into double volume of 0.25% PVA and stirred for 4 hours in open air to evaporate organic solvents. The samples were kept away from light if fluorescent dye was added instead of tetracycline. Low speed centrifugation (3,000 round per minute/rpm, 5 minutes) was performed to remove undesired

clumps; and then ultracentrifugation at 17,000 g for 15 minutes was done twice to wash and precipitate the NPs. PLGA NPs were resuspended in 5 ml Millipore water and stored in 4°C fridge. When 20% GelMA with NPs and SiMPs was prepared, the full formulation contained 500 μl of PLGA NPs, 10 mg of cytokine loaded SiMPs and 500 μl of 40% GelMA, which were mixed evenly.

Mesoporous silica particle preparation.

Monodisperse mesoporous SiMPs were formed by using a microfluidic jet spray-drying route, using cetyltrimethylammonium bromide (CTAB) and/or Pluronic F127 as templating agents and tetraethylorthosilicate (TEOS) for silica as reported before.[26,27] Carbodiimide chemistry (NHS/EDC) was utilized to link heparin to SiMPs after treating the silica with (3-Aminopropyl)triethoxysilane (APTES) to provide primary amine groups. Briefly, 800 mg SiMPs were suspended in 50 ml dehydrated Methanol. Then, 3 ml APTES was added, and the suspension was stirred at room temperature overnight, and the final product was centrifuged at 1500 rpm for 3 minutes and washed with methanol three times, followed by drying under high vacuum overnight. For the surface functionalization of the aminated-silica particles with heparin sodium salt following activation *via* successive addition of EDC and NHS. After activation for 10 minutes, the ethanolic solution of amino-functionalized silica was added to the reaction mixture and stirred for 12 hours at room temperature. Afterwards the particles were separated by centrifugation at 1500 rpm for 3 minutes and washed several times with deionized water and ethanol to remove unreacted reagents.

The hydrolysis of heparin-coated mesoporous silica structure (without cytokines) was used to estimate the degradation rate of SiMPs. To study in vitro degradation, SiMPs were soaked in RPMI medium supplemented with 10% heat-inactivated fetal bovine serum, 1% penicillin/streptomycin, 1% sodium pyruvate, 1% HEPES buffer, and 0.1% μM beta-mercaptoethanol. The supernatant was collected from the pelleted SiMPs at designated timepoints, and tested with inductively coupled plasma mass spectrometry (ICP-MS; NexION 2000, PerkinElmer) to estimate the atomic content of silicon, which was then normalized to the initial mass to estimate the remaining mass. *IL-4 and TGF-β loading into the silica particles.* First, SiMPs were activated by 3-aminopropyltrimethoxysilane (APTES), and 800 mg of SiMPs was suspended in 50 mL of methanol. Then, 3 mL of APTES was added and suspension was stirred at room temperature overnight; the final product was centrifuged (1500 rpm, 3 minutes), washed with methanol five times, and dried under high vacuum. Secondly, aminated-SiMP surfaces were functionalized with heparin, and 216 mg of heparin sodium salt were dissolved in 8 mL deionized H_2O. Then, 62.1 mg EDC and 70.4 mg sulfoNHS were added successively and stirred for 5 minutes at room temperature. The amount of 1.12 mL ethanolic solution with 20 mg of the amino-functionalized SiMPs was added to the reaction mixture and stirred overnight at room temperature. Afterwards the particles were separated by centrifugation and washed several times with copious amounts of water and ethanol to remove additional free polysaccharide. They were re-dispersed in 5 mL ethanol, leading to a colloidal solution. Thirdly, heparin-modified SiMPs were incubated with 1 μg of IL-4 and 1 μg of TGF-β for cytokine loading overnight. Afterwards the microparticles were centrifuged down using tabletop centrifuge and washed three times with PBS to remove free cytokines.

MN patch fabrication.

To fabricate MNs, 20% GelMA containing 0.5% photoinitiator, tetracycline-loaded NPs and IL-4/TGF-β-loaded SiMPs were casted on negative MN molds and centrifuged at 3,000 rpm for 2 minutes. The GelMA mixture was maintained at the temperature greater than 50°C throughout the procedures in order to maintain the material fluidity, but the duration of elevated temperature was minimized to protect protein integrity. Extra mixture was removed, and then 100 μl of 10% gelatin containing 5 mg/ml of tetracycline-HCl was laid evenly on the top to create a 1 cm × 1 cm patch. The MN patches were incubated under 50W/cm^2 ultraviolet light for 5 minutes. After 1 day of drying in dark at room temperature, solidified MN patches were peeled off from the molds and stored at 4°C until use.

Mechanical property of MNs.

The mechanical strength of MNs was measured by compression test on a low-force mechanical testing system (5943 MicroTester, Instron, USA). The MN tips were place perpendicularly to stainless-steel plate and were pressed against another stainless-steel plate moving at constant speed of 0.5 mm/minutes. Correlations between the applied force and the deformation of the MNs were recorded. All tests were performed in triplicates.

Tetracycline release study.

In vitro release of tetracycline was studied by incubating a single patch in 1 mL PBS (pH 7.4; supplemented with 10 mM $CaCl_2$) at 37°C under constant gentle stirring. At different time intervals, stirring was stopped and 1 μL of the supernatant was taken from the sample. The concentration of released tetracycline was determined by measuring the absorbance at 270 nm wavelength using UV-vis spectrophotometer (Thermo Scientific NanoDrop One).

Antibacterial assay.

Kirby-Bauer agar disk diffusion assay was used to test antibacterial properties of tetracycline loaded MNs against *E. Coli* and *A.a*. A free drug control was prepared by adding tetracycline solution to 8mm sterile paper disks. These paper disks were air-dried in a biosafety cabinet before use. These disks and MN patches were placed in agar plates inoculated with bacteria at 37°C. The inhibition zones were measured after 48 hours.

Animal studies.

Five- to seven-week-old wild-type (C57Bl/6) mice were purchased from the Jackson Laboratory and maintained in specific pathogen-free facilities at the University of California at Los Angeles (UCLA). All experiments on mice and cells collected from mice were performed under a protocol approved by the Animal Research Committee and in accordance with UCLA's institutional policy on humane and ethical treatment of animals.

T-cell isolation and activation.

Primary T cells and $CD4^+$ T cells were isolated from mouse spleen and purified using magnetic-based, negative enrichment kits (Stem Cell Technologies). Cells were counted by hemocytometer using trypan blue exclusion (Calbiochem). RPMI medium supplemented with 10% heat-inactivated fetal bovine serum, 1% penicillin/streptomycin, 1% sodium

pyruvate, 1% HEPES buffer, and 0.1% μM beta-mercaptoethanol was used as T-cell culture media. For experiments to induce Treg, $CD4^+$ T cells were purified from mouse spleens by EasySep immunomagnetic negative selection (Stem Cell Technologies). Cells were then activated with anti-CD3 antibody (10 μg/mL)-coated plates supplemented with anti-CD28 antibody (2 μg/mL) in medium. At the same time, MNs loaded with cytokines (IL-4, and TGF-β) were added. After four days, cells were removed from wells and fixed, permeabilized, and stained with anti-CD25 and intracellular anti-Foxp3 antibodies for flow cytometry analysis of Tregs.

Isolation of bone-marrow derived macrophages (BMDMs).

5-to-7-week-old C57Bl/6 mice were euthanized, and hind limbs were harvest in PBS. Under sterile condition, muscles were scraped off and the ends of bones were cut off. Bone marrow was flushed into a sterile 50-ml conical tube with 2 ml of Dulbecco's Modified Eagle Medium (DMEM)/F12 supplemented with 10% fetal bovine serum and 1% penicillin-streptomycin. Cells were pelleted and plated with mouse 50 ng/ml macrophage colony-stimulating factor (BioLegend). Following 3 days of incubation, 5 ml of fresh complete DMEM/F12 medium with 25 ng/ml macrophage colony-stimulating factor were supplied per 10-cm cell culture dish. Cells were again incubated for 3 more days. Then supernatants were discarded, and dishes were washed with PBS three times to remove non-adherent cells. BMDMs were gently scraped off the dish, pelleted, counted and seeded in new plates for further macrophage polarization and experimentation. 10 ng/ml LPS was used to induce proinflammatory macrophages, while 25 ng/ml IL-4 was used to induce pro-healing macrophages. Controls were simply adding complete DMEM/F12 medium.

RNA isolation, reverse transcription and qPCR.

Total RNA was extracted by using TRIzol reagent (Life Technologies, Gaithersburg, MD, U.S.A.), and the concentration was determined from spectrophotometric optical density measurement (Thermo Scientific NanoDrop). The OD260/OD280 ratio in all samples ranged between 1.7 and 2.0 to ensure RNA purity. Reverse transcription was then carried out using Maxima SYBR Green qPCR master mix according to manufacturer's suggested protocol. The cDNA was stored at −20°C. PCR was performed by using SYBR Green kit according to manufacturer's suggested protocol on BioRad CFX96 PCR detection system. Primer sequences were as follow: GAPDH- Forward 5'CATCACTGCCACCCAGAAGACTG Reverse 5' ATGCCAGTGAGCTTCCCGTTCAG; iNOS – Forward 5' GAGACAGGGAAGTCTGAAGCAC Reverse 5'CCAGCAGTAGTTGCTCCTCTTC; IL-1 – Forward 5' TGGACCTTCCAGGATGAGGACA Reverse 5' GTTCATCTCGGAGCCTGTAGTG; MRC1 – Forward 5'GTTCACCTGGAGTGATGGTTCTC Reverse 5' AGGACATGCCAGGGTCACCTTT; ARG-1 – Forwards 5' CATTGGCTTGCGAGACGTAGAC; Reverse 5' GCTGAAGGTCTCTTCCATCACC.

Animal study.

In vivo functionality of designed MNs was evaluated using a rat periodontal defect model, as described previously with some modifications [32,34]. Two-month-old virgin male and

female Sprague Dawley rats (Harlan Laboratories, Livermore, CA) were utilized for *in vivo* testing of the proposed periodontal treatments according to approved animal protocols. The animals were divided into four groups (four rats per group): (i) healthy control, (ii) no treatment (untreated), (iii) blank MN patches, and (iv) therapeutic MN patches containing tetracycline and cytokines. Briefly, mucoperiosteal flaps were elevated in rats in groups (ii-iv), uncovering the alveolar bone adjacent to the mesiolingual aspect of the first maxillary molars. The alveolar bone covering the root surfaces on the lingual side was removed with a dental bur under constant saline irrigation, and *A.a.*-coated 5–0 silk ligature was tied around the left second molar. Silk ligature was inoculated with *A.a.* under anaerobic conditions for 24 hours before the procedure. Three weeks later, designed patches were inserted into the defect site as noted above for groups. Eight weeks post-implantation, the animals were sacrificed and the amounts of bone regeneration at defect sites were evaluated using μCT analysis. All the specimens were standardized, and μCT images were calibrated for proper comparative analysis. The vertical bone loss at each defect site was evaluated by measuring the distance between cementoenamel junction (CEJ) and alveolar bone crest as well as the relative alveolar bone area according to methods reported in the literature.[33]

Characterization of inflammatory response at defect sites.

Populations of immune cells in periodontal tissue were analyzed as described previously [34]. Briefly, at 8 weeks post-implantation, buccal and palatal tissues of maxillary molars were isolated and dissociated using collagenase and DNase I (50 μg/mL) at 37°C for 15 minutes. These enzymes were then inactivated with EDTA (20 μL/mL of solution). Tissues were then disaggregated and passed through a 100-μm cell strainer to obtain a single-cell suspension. Quantitative PCR assays were used to analyze gene expression. RNA from isolated cells was isolated using Trizol reagent. RNA was reverse-transcribed and single-stranded cDNA was made using a Superscript III cDNA synthesis kit. Relative gene expression was calculated using the $2^{-\Delta\Delta Ct}$ method, with normalization to the *Ct* of the housekeeping gene beta actin. Quantification of *A.a.* in the periodontal tissues was performed as previously reported [34]. The concentrations of inflammatory cytokines and anti-inflammatory cytokines were measured by using ELISA kits after the extraction of proteins from the gingival tissue by tissue homogenization.

Statistical analysis.

The Kruskal-Wallis rank sum test, one-way ANOVA and two-tailed Student's t-test were utilized as appropriate to analyze the data at a significance of α or $p < 0.05$. Quantitative data are expressed as mean ± SD. To determine the number of specimens for the proposed experiments, power analysis was conducted based on our preliminary data.

Supplementary Material

Refer to Web version on PubMed Central for supplementary material.

Acknowledgements

This work is supported in part by grants from the National Institute of Dental & Craniofacial Research (R56DE029157), Center for Dental, Oral and Craniofacial Tissue Organ Regeneration (U24 DE026914), and Eli

and Edythe Broad Center of Regenerative Medicine and Stem Cell Research Award Program. The contents of this publication are solely the responsibility of the authors and do not necessarily represent the official views of NIH, or/and other agency of the State of California.

REFERENCES

1. Pihlstrom BL, Michalowicz BS, and Johnson NW (2005). Periodontal diseases. Lancet 366, 1809–1820. [PubMed: 16298220]
2. Dye B, Thornton-Evans G, Li X, and Iafolla T (2015). Dental caries and tooth loss in adults in the United States, 2011–2012. NCHS Data Brief, 197.
3. Chen F-M, Zhang J, Zhang M, An Y, Chen F, and Wu Z-F (2010). A review on endogenous regenerative technology in periodontal regenerative medicine. Biomaterials 31, 7892–7927. [PubMed: 20684986]
4. Patel SK, Greene AC, Desai SM, Rothstein S, Basha IT, MacPherson JS, Wang Y, Zou Y, Shehabeldin M, Sfeir CS, et al. (2021). Biorelevant and screening dissolution methods for minocycline hydrochloride microspheres intended for periodontal administration. Int. J. Pharm. 596, 120261. [PubMed: 33486044]
5. Khaliq NU, Chobisa D, Richard CA, Swinney MR, and Yeo Y (2021). Engineering microenvironment of biodegradable polyester systems for drug stability and release control. Ther. Deliv. 12, 37–54. [PubMed: 33397135]
6. Graves D (2008). Cytokines that promote periodontal tissue destruction. J. Periodontol. 79, 1585–1591. [PubMed: 18673014]
7. Kayal RA (2013). The role of osteoimmunology in periodontal disease. Biomed Res. Int. 2013, 639368. [PubMed: 24151615]
8. Mantovani A, Biswas SK, Galdiero MR, Sica A, and Locati M (2013). Macrophage plasticity and polarization in tissue repair and remodelling. J. Pathol. 229, 176–185. [PubMed: 23096265]
9. Benoit M, Desnues B, and Mege J-L (2008). Macrophage polarization in bacterial infections. J. Immunol. 181, 3733–3739. [PubMed: 18768823]
10. Alvarez C, Suliman S, Almarhoumi R, Vega ME, Rojas C, Monasterio G, Galindo M, Vernal R, and Kantarci A (2020). Regulatory T cell phenotype and anti-osteoclastogenic function in experimental periodontitis. Sci. Rep. 10, 19018. [PubMed: 33149125]
11. Wang N, Liang H, and Zen K (2014). Molecular mechanisms that influence the macrophage m1-m2 polarization balance. Front. Immunol. 5, 614. [PubMed: 25506346]
12. Murray PJ, Allen JE, Biswas SK, Fisher EA, Gilroy DW, Goerdt S, Gordon S, Hamilton JA, Ivashkiv LB, Lawrence T, et al. (2014). Macrophage activation and polarization: nomenclature and experimental guidelines. Immunity 41, 14–20. [PubMed: 25035950]
13. Raimondo TM, and Mooney DJ (2018). Functional muscle recovery with nanoparticle-directed M2 macrophage polarization in mice. Proc. Natl. Acad. Sci. U. S. A. 115, 10648–10653. [PubMed: 30275293]
14. Yang W-C, Hwang Y-S, Chen Y-Y, Liu C-L, Shen C-N, Hong W-H, Lo SM, and Shen C-R (2017). Interleukin-4 supports the suppressive immune responses elicited by regulatory T cells. Front. Immunol. 8, 1508. [PubMed: 29184551]
15. Mokarram N, Dymanus K, Srinivasan A, Lyon JG, Tipton J, Chu J, English AW, and Bellamkonda RV (2017). Immunoengineering nerve repair. Proc. Natl. Acad. Sci. U. S. A. 114, E5077–E5084. [PubMed: 28611218]
16. Stadler AF, Angst PDM, Arce RM, Gomes SC, Oppermann RV, and Susin C (2016). Gingival crevicular fluid levels of cytokines/chemokines in chronic periodontitis: a meta-analysis. J. Clin. Periodontol. 43, 727–745. [PubMed: 27027257]
17. Cekici A, Kantarci A, Hasturk H, and Van Dyke TE (2014). Inflammatory and immune pathways in the pathogenesis of periodontal disease. Periodontol. 2000 64, 57–80.
18. Hajishengallis G, and Korostoff JM (2017). Revisiting the Page & Schroeder model: the good, the bad and the unknowns in the periodontal host response 40 years later. Periodontol. 2000 75, 116–151.

19. Pan W, Wang Q, and Chen Q (2019). The cytokine network involved in the host immune response to periodontitis. Int. J. Oral Sci. 11, 30. [PubMed: 31685798]
20. Prausnitz MR (2017). Engineering Microneedle patches for vaccination and drug delivery to skin. Annu. Rev. Chem. Biomol. Eng. 8, 177–200. [PubMed: 28375775]
21. Lee K, Goudie MJ, Tebon P, Sun W, Luo Z, Lee J, Zhang S, Fetah K, Kim H-J, Xue Y, et al. (2020). Non-transdermal microneedles for advanced drug delivery. Adv. Drug Deliv. Rev. 165–166, 41–59.
22. Xu C, Lei C, and Yu C (2019). Mesoporous silica nanoparticles for protein protection and delivery. Front. Chem. 7, 290. [PubMed: 31119124]
23. Luo Z, Sun W, Fang J, Lee K, Li S, Gu Z, Dokmeci MR, and Khademhosseini A (2019). Biodegradable gelatin methacryloyl microneedles for transdermal drug delivery. Adv. Healthc. Mater. 8, e1801054. [PubMed: 30565887]
24. Schirmer L, Atallah P, Werner C, and Freudenberg U (2016). StarPEG-heparin hydrogels to protect and sustainably deliver IL-4. Adv. Healthc. Mater. 5, 3157–3164 [PubMed: 27860466]
25. Majedi FS, Hasani-Sadrabadi MM, Kidani Y, Thauland TJ, Moshaverinia A, Butte MJ, Bensinger SJ, and Bouchard L-S (2018). Cytokine secreting microparticles engineer the fate and the effector functions of T-cells. Adv. Mater. 30, 1703178.
26. Waldron K, Wu WD, Wu Z, Liu W, Selomulya C, Zhao D, and Chen XD (2014). Formation of monodisperse mesoporous silica microparticles via spray-drying. J. Colloid Interface Sci. 418, 225–233 [PubMed: 24461839]
27. Liu W, Chen XD, and Selomulya C (2015). On the spray drying of uniform functional microparticles. Particuology. 22, 1–12
28. Orecchioni M, Ghosheh Y, Pramod AB, and Ley K (2019). Macrophage polarization: different gene signatures in M1(LPS+) vs. classically and M2(LPS−) vs. alternatively activated macrophages. Front. Immunol. 10, 1084. [PubMed: 31178859]
29. Stein M, Keshav S, Harris N, and Gordon S (1992). Interleukin 4 potently enhances murine macrophage mannose receptor activity: a marker of alternative immunologic macrophage activation. J. Exp. Med. 176, 287–292. [PubMed: 1613462]
30. Josefowicz SZ, Lu L-F, and Rudensky AY (2012). Regulatory T cells: mechanisms of differentiation and function. Annu. Rev. Immunol. 30, 531–564. [PubMed: 22224781]
31. Chen W, Jin W, Hardegen N, Lei K-J, Li L, Marinos N, McGrady G, and Wahl SM (2003). Conversion of peripheral CD4+CD25− naive T cells to CD4+CD25+ regulatory T cells by TGF-beta induction of transcription factor Foxp3. J. Exp. Med. 198, 1875–1886. [PubMed: 14676299]
32. Hasani-Sadrabadi MM, Sarrion P, Nakatsuka N, Young TD, Taghdiri N, Ansari S, Aghaloo T, Li S, Khademhosseini A, Weiss PS, et al. (2019). Hierarchically patterned polydopamine-containing membranes for periodontal tissue engineering. ACS Nano 13, 3830–3838. [PubMed: 30895772]
33. Hasani-Sadrabadi MM, Sarrion P, Pouraghaei S, Chau Y, Ansari S, Li S, Aghaloo T, and Moshaverinia A (2020). An engineered cell-laden adhesive hydrogel promotes craniofacial bone tissue regeneration in rats. Sci. Transl. Med. 12.
34. Glowacki AJ, Yoshizawa S, Jhunjhunwala S, Vieira AE, Garlet GP, Sfeir C, and Little SR (2013). Prevention of inflammation-mediated bone loss in murine and canine periodontal disease via recruitment of regulatory lymphocytes. Proc. Natl. Acad. Sci. 110, 18525–18530. [PubMed: 24167272]
35. Prakasam A, Elavarasu SS, and Natarajan RK (2012). Antibiotics in the management of aggressive periodontitis. J. Pharm. Bioallied Sci. 4, S252–5. [PubMed: 23066264]

Progress and Potential statement

Periodontitis is a prevalent chronic inflammatory disease causing the degeneration of tooth-supporting tissues in humans. To combat this disease, oral administration of antibiotics is a conventional strategy. However, the critical role of immune cells has not been addressed for therapeutic development. To address the challenge of drug delivery in oral cavity and achieve periodontal tissue regeneration, we engineer an immunomodulatory microneedle patch to enable minimally invasive tissue penetration and local retention for a sustained delivery of antibiotics and cytokines. The modular design of microneedle patch with tunable degradation rates of base, needles, nanoparticles and microparticles can be adapted as a drug delivery platform for broad applications. This immunoengineering approach may inspire innovative local immunotherapies for disease treatment and tissue regeneration.

Highlights

- Modular MN patch allows a multi-stage and controlled release of therapeutic drugs
- Dual delivery of antibiotic and cytokines modulates local immune cells
- Local immunomodulation promotes pro-regenerative signals for tissue repair

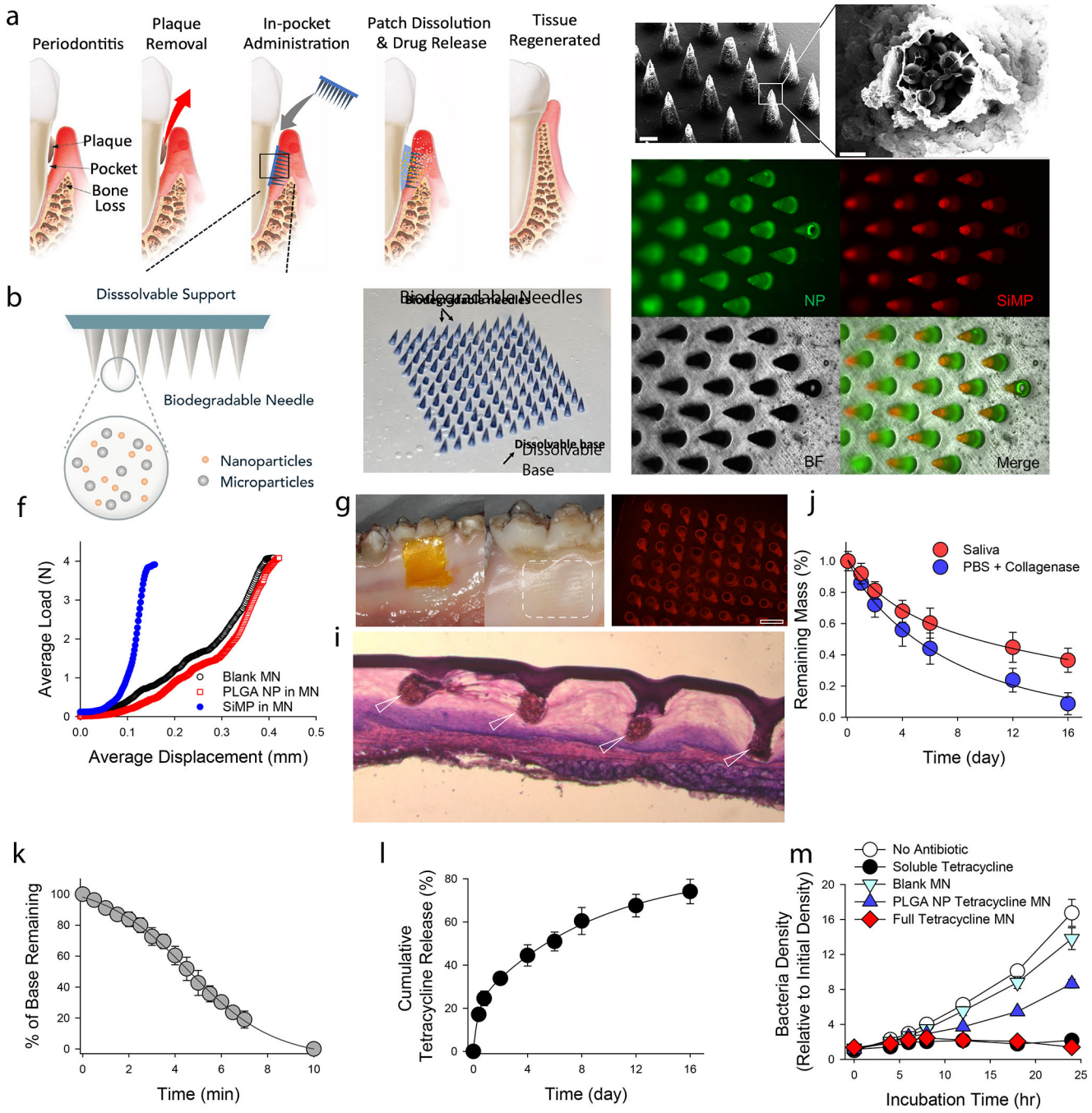

Figure 1. Physical and chemical characterization of MN patches.

a, Proposed working mechanism of the designed immunotherapeutic periodontal MN patch. MN patches are designed to provide transgingival administration of antibiotics and anti-inflammatory cytokines. Following administration, MNs will detach from the supporting membrane upon gelatin dissolution and stay in gingival tissue, release their cargos, and degrade. **b**, Illustration of the multifunctional MN patch design. The image on the right shows an example of fabricated MN patch. MNs were visualized by encapsulating Trypan Blue dye. **c**, Scanning electron microscopy (SEM) image of fabricated MNs. **d**,

Encapsulated SiMPs can be seen inside truncated needles. See also Figure S2. **e**, Fluorescent imaging demonstrates the distribution of fluorophore-conjugated PLGA NPs (in Green) and SiMPs (in Red) inside GelMA-based MNs. **f**, Mechanical strength of MNs measured by Instron compression test. **g**, MN patch penetrated on freshly harvested porcine gingiva. Following the administration, the tissue was kept in 37°C incubator for 30 minutes to monitor gelatin dissolution. Pig's gingival surface is showing insertion of MNs. **h**, MN-treated pig gingival tissue was imaged to demonstrate the presence of fluorophore-loaded MNs (in Red). Scale bar: 400 μm. **i**, Penetration of MN into fresh rat gingival tissue was visualized by hematoxylin and eosin (H&E) staining. **j**, *In vitro* degradation of MNs over time in PBS containing collagenase enzyme or human saliva at 37°C under gentle shaking. **k**, FITC-conjugated gelatin was used as the support layer to measure the rate of gelatin base dissolution. **l**, Cumulative *in vitro* release of tetracycline was assessed from the dissolution of gelatin base (burst release) and from GelMA MNs loaded with PLGA-tetracycline NPs (sustained release) at 37°C and pH 7.4. **m,** Antibacterial effect of designed patches against *P.g.* Full tetracycline MN includes tetracycline-loaded gelatin base and tetracycline-loaded PLGA NPs in MNs. The data in **j-m** are presented as mean ± standard deviation (SD) (n = 5).

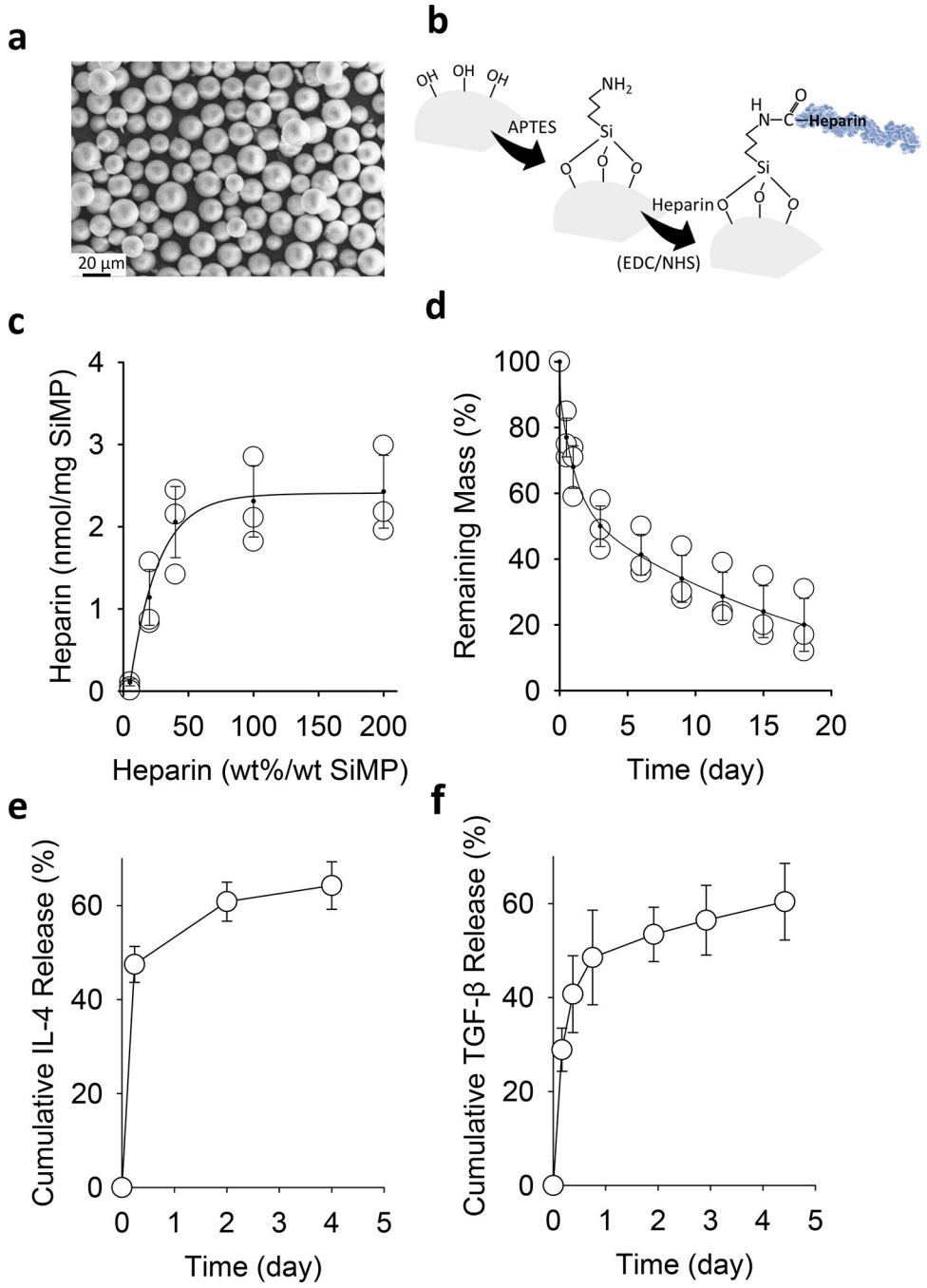

Figure 2. Sustained release of IL-4 and TGF-β from silica-heparin microparticles.

a, SEM image of mesoporous SiMPs. **b**, Surface chemistry to functionalize SiMP surface with heparin. **c**, The efficiency of heparin-conjugation on SiMPs with various initial amounts of heparin in the reaction mixture. **d**, *In vitro* degradation of heparin-functionalized SiMPs over time. **e-f,** Cumulative release of IL-4 **(e)** and TGF-β **(f)** from heparin-functionalized SiMPs at 37°C. The data are presented as mean ± SD (n = 5).

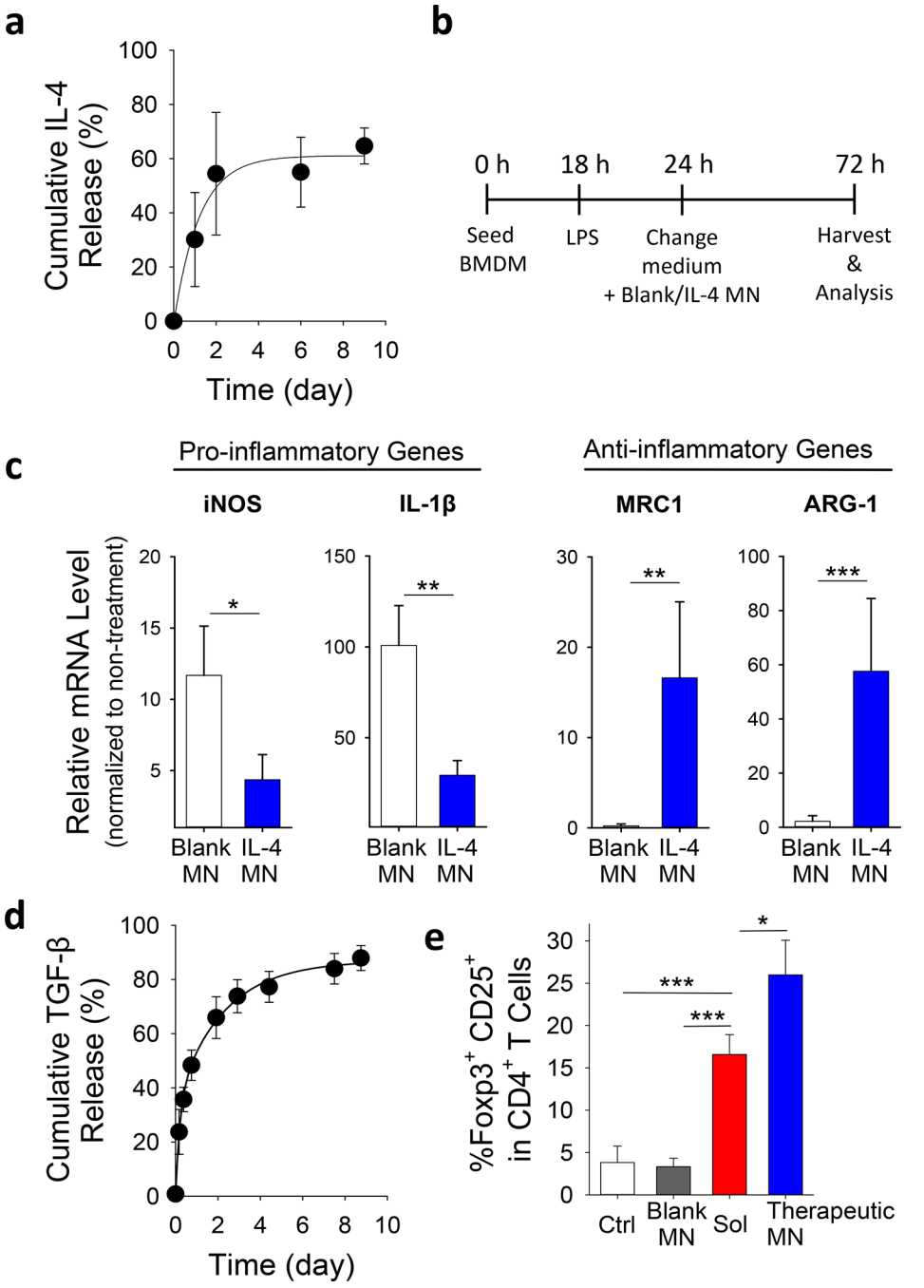

Figure 3. Immunomodulatory properties of MN patches *in vitro*.

a, Cumulative *in vitro* release of IL-4 from MN patches containing IL-4-loaded SiMPs at 37°C and pH 7.4. **b**, Experiment procedure of co-culturing LPS-treated BMDMs with MN patches. **c**, Effects of IL-4 released from MN patches on the gene expression of pro/anti-inflammatory markers in LPS-treated BMDMs as assessed by using qPCR. See also Figure S9 for results from no-contact setup. **d**, Cumulative *in vitro* release of TGF-β from MN patches containing TGF-β-loaded SiMPs at 37°C and pH 7.4. **e**, Effects of MN-released IL-4/TGF-β on the development of induced Treg. Naïve $CD4^+$ T-cells were treated with

anti-CD3 and anti-CD28 antibodies for 4 days in the presence of IL-4/TGF-β in solution (Sol), blank MN patches or MN patches with IL-4/TGF-β (Therapeutic MN), followed by flow cytometric analysis of Treg development (co-expression of Foxp3 and CD25). All data are presented as mean ± SD (n = 5). The results were analyzed using one-way ANOVA with post-hoc analysis. Statistical significance is indicated by * $p < 0.05$, ** $p < 0.01$ and *** $p < 0.001$.

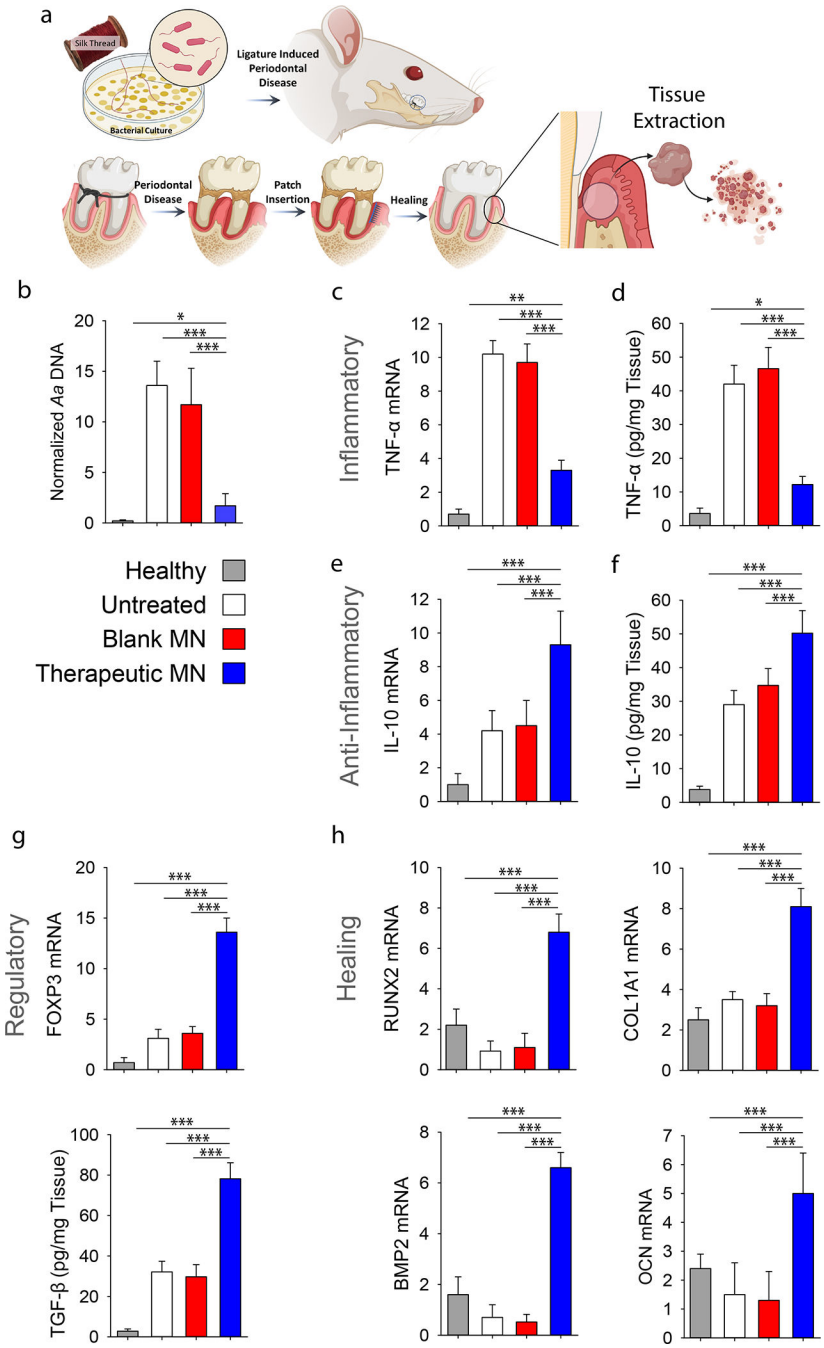

Figure 4. *In vivo* evaluation of the immunomodulatory effects in a rat model of periodontitis.

a, Ligature induced periodontal disease model in rats was used. **a**, Schematic representation of the proposed disease induction strategy patch placement. Mucoperiosteal flaps were elevated, uncovering the alveolar bone adjacent to the lingual aspect of the first maxillary molar to place MN at the defect site. At 8-weeks post MN insertion, buccal and palatal tissues of maxillary molars were isolated and dissociated to assess inflammatory status of tissue microenvironment. **b**, PCR analysis of *A.a.* bacterial ribosomal DNA in the periodontal tissue normalized by palatal tissue weight. **c**, Relative mRNA expression level of

pro-inflammatory cytokine TNF-α. See also Figure S10. **d**, ELISA analysis of TNF-α level in the tissue. **e**, Relative mRNA expression level of anti-inflammatory cytokine IL-10. **f**, ELISA analysis of IL-10 in the tissue. **g,** Relative mRNA expression of Treg marker FOXP3 and ELISA analysis of TGF-β secretion. **h**, Relative mRNA expression level pro-healing genes RUNX2, COL1A1, BMP2 and OCN in the periodontal tissue. Healthy: healthy rats; Untreated: untreated periodontitis; Blank MN: MN patches without any therapeutic cargo; Therapeutic MN: MN patches containing both tetracycline- and IL-4/TGF-β-loaded SiMPs (Tetracycline: 0.5 mg; IL-2: 100 ng, IL-4: 40 ng, and TGF-β: 40 ng per patch). The presented data are expressed as mean ± SD (n= 5). The results were analyzed by using one-way ANOVA with post-hoc analysis. Statistical significance is indicated by * $p < 0.05$, ** $p < 0.01$ and *** $p < 0.001$.

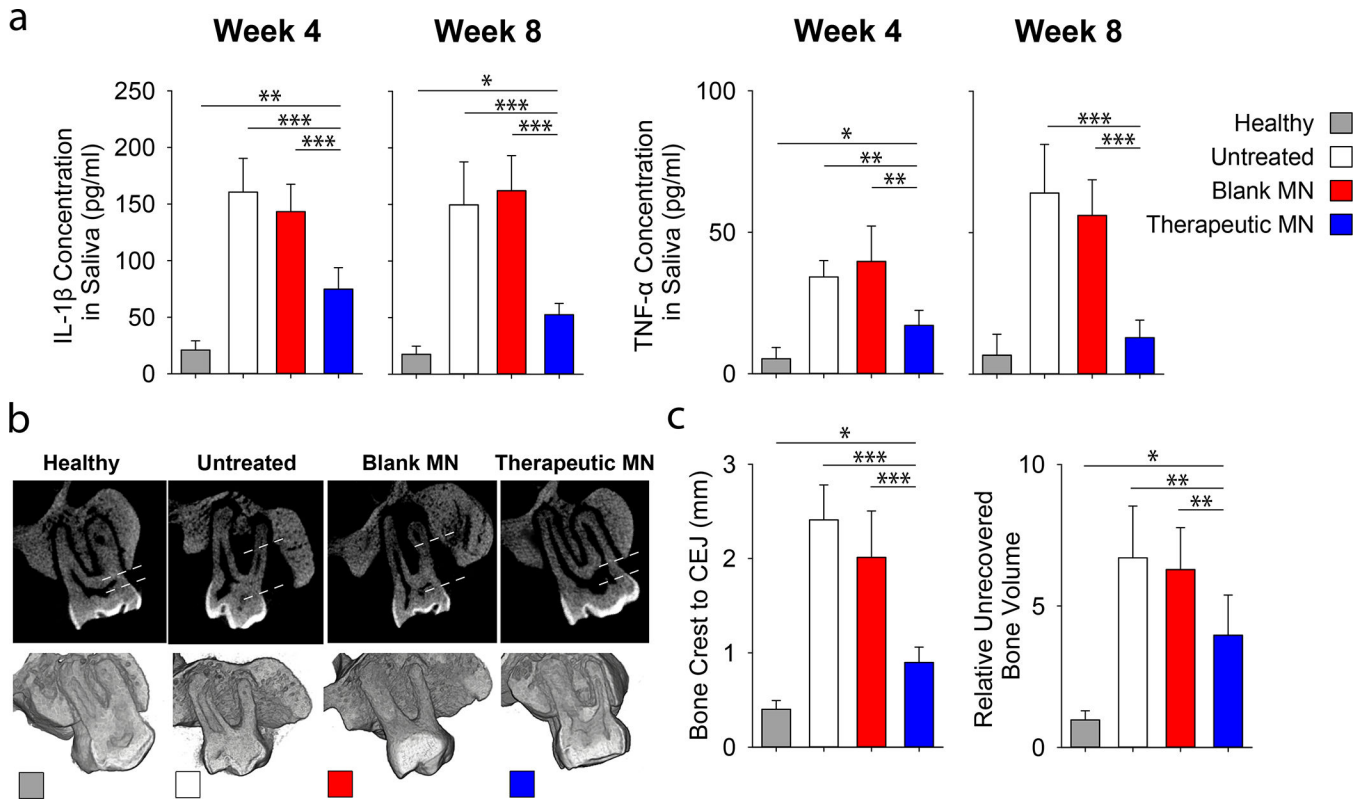

Figure 5. Effects of therapeutic MN patches on the regeneration of periodontal tissue *in vivo*.

Ligature induced periodontal disease model in rats was used. **a**, Quantification of inflammatory (TNF-α and IL-1β) cytokines in rat saliva at 4- and 8-weeks post MN implantation. **b**, The μCT images of the rat maxilla at 8 weeks post MN implantation. All specimens were normalized, and μCT images were calibrated to enable quantitative comparisons. Dotted line indicated the distances between bone crest and CEJ. **c**, Quantitative analysis of the vertical bone recovery as determined by measuring the distance between the bone crest and CEJ after 8-weeks of treatment. **d**, Relative volumetric bone recovery was calculated by using 3D reconstructed volume at 8 weeks post MN implantation. All data are presented as mean ± SD (n= 5). Statistical significance is indicated by * $p < 0.05$, ** $p < 0.01$ and *** $p < 0.001$ for differences between samples with different formulations.